

Goethe-Universität Frankfurt am Main

Fachbereich 13

ITP - Institut für Theoretische Physik

Bachelor Thesis

Low-lying Energy Eigenstates of a Static $Q\bar{Q}$ Pair in a Periodic Spatial Volume

---

Elias Siegert

Submitted on September 29, 2026

First supervisor:
Prof. Dr. Marc Wagner

Second supervisor:
Prof. Dr. Owe Philipsen

Abstract

We study the two lowest energy levels of a static quark-antiquark pair in SU(2) Yang-Mills theory on a lattice with periodic boundary conditions, where one spatial direction is shortened. Due to the periodicity the gluonic flux tube between the static charges can connect the pair either directly or by wrapping around the shortened direction. This gives two string states, which are degenerate when the pair is separated by half the shortened extent, as both paths then have the same length. The shortened direction acts like an inverse temperature, so that reducing its extent drives this direction from the confined into the deconfined phase. We generate gauge configurations with Monte Carlo simulations at the inverse gauge coupling $\beta = 2.40$, corresponding to a lattice spacing $a \approx 0.10$ fm, with an extent of $24a$ in the other directions and shortened extents of $8a$, $6a$ and $4a$. On these we compute correlation matrices from the direct and the wrapped Wilson line and solve a generalized eigenvalue problem. We find that the mixing of both states is controlled by the Z_2 center symmetry, whose breaking signals deconfinement. In the confined phase the off-diagonal elements of the correlation matrix vanish and the two lowest levels cross sharply, while in the deconfined phase the states mix and form an avoided level crossing with a splitting of about $a\Delta E \approx 0.45$. We locate the critical extent between $4a$ and $6a$, i.e. between about 0.4 fm and 0.6 fm.

Zusammenfassung

Wir untersuchen die beiden niedrigsten Energieniveaus eines statischen Quark-Antiquark-Paares in der SU(2)-Yang-Mills-Theorie auf einem Gitter mit periodischen Randbedingungen, auf dem eine räumliche Richtung verkürzt ist. Aufgrund der Periodizität kann der gluonische Flussschlauch zwischen den statischen Ladungen das Paar entweder direkt oder um die verkürzte Richtung herumlaufend verbinden. Dies ergibt zwei Stringzustände, die entartet sind, wenn das Paar um die halbe verkürzte Ausdehnung getrennt ist, da beide Wege dann die gleiche Länge haben. Die verkürzte Richtung wie eine inverse Temperatur wirkt, daher führt eine Verringerung ihrer Ausdehnung diese Richtung von der Confinement- in die Deconfinement-Phase. Wir erzeugen Eichfeldkonfigurationen mit Monte-Carlo-Simulationen bei der inversen Eichkopplung $\beta = 2{,}40$, entsprechend einem Gitterabstand $a \approx 0{,}10$ fm, mit einer Ausdehnung von $24a$ in den anderen Richtungen und verkürzten Ausdehnungen von $8a$, $6a$ und $4a$. Auf diesen berechnen wir Korrelationsmatrizen aus der direkten und der umlaufenden Wilson-Linie und lösen ein verallgemeinertes Eigenwertproblem. Wir finden, dass die Mischung beider Zustände durch die Z_2-Zentrumssymmetrie bestimmt wird, deren Brechung Deconfinement anzeigt. In der Confinement-Phase verschwinden die Nebendiagonalelemente der Korrelationsmatrix und die beiden niedrigsten Niveaus kreuzen sich scharf, während in der Deconfinement-Phase die Zustände mischen und eine vermiedene Niveaukreuzung mit einer Aufspaltung von etwa $a\Delta E \approx 0{,}45$ bilden. Wir bestimmen die kritische Ausdehnung zwischen $4a$ und $6a$, also zwischen etwa 0,4 fm und 0,6 fm.

Selbstständigkeitserklärung

Erklärung nach § 39 (15) Prüfungsordnung 2020 für den BAMA-Studiengang Physik

Hiermit erkläre ich, dass ich die Arbeit selbstständig und ohne Benutzung anderer als der angegebenen Quellen und Hilfsmittel verfasst habe. Alle Stellen der Arbeit, die wörtlich oder sinngemäß aus Veröffentlichungen oder aus anderen fremden Texten entnommen wurden, sind von mir als solche kenntlich gemacht worden. Ferner erkläre ich, dass die Arbeit nicht - auch nicht auszugsweise - für eine andere Prüfung verwendet wurde. Zur sprachlichen Überarbeitung des Textes und zur Überprüfung des Analysecodes wurden KI-basierte Werkzeuge verwendet. Alle physikalischen Inhalte, Simulationen und Ergebnisse stammen von mir.

Ort, Datum: ..... Unterschrift: .....

Contents

1 Introduction **1**

2 Theoretical Framework **2**
2.1. Conventions and Notation . . . 2
2.2. Wilson Loops and the Static Potential . . . 2
2.3. Polyakov Loops and Center Symmetry . . . 4
2.3.1. Center Transformations . . . 5
2.3.2. The Polyakov Loop as an Order Parameter . . . 5
2.4. The Static $Q\bar{Q}$ Pair in a Periodic Volume . . . 6
2.4.1. Direct and Wrapped Wilson Lines . . . 7
2.4.2. Correlation Matrix . . . 7
2.4.3. Confinement Constraints on the Off-Diagonal Elements . . . 8
2.5. Expected Spectrum . . . 9
2.5.1. Sharp Level Crossing in Confinement . . . 9
2.5.2. Sector Selection and Avoided Level Crossing . . . 10
2.5.3. Further Excited States at Small Separations . . . 10

3 Simulation and Analysis Methods **12**
3.1. Gauge Field Generation and Smearing . . . 12
3.2. Generalized Eigenvalue Problem . . . 13
3.3. Statistical Analysis . . . 14
3.4. Scale Setting . . . 15

4 Numerical Results **16**
4.1. Off-Diagonal Elements and Center Symmetry . . . 16
4.2. Energy Spectrum along the Shortened Direction . . . 17
4.2.1. Confined Extent $l = 8a$ . . . 17
4.2.2. Near-Critical Extent $l = 6a$ . . . 18
4.2.3. Deconfined Extent $l = 4a$ . . . 19
4.3. The Level Splitting at $r = \frac{l}{2}$ . . . 20
4.4. The Excited State at Large Extents . . . 21

5 Conclusion and Outlook **22**
5.1. Conclusion . . . 22
5.2. Outlook . . . 23

A Thermalization **24**

B Effective Energy Plateaus **26**

Bibliography **28**

Chapter 1

Introduction

Confinement is a fundamental property of quantum chromodynamics. It is the reason why colored charges are never observed in isolation, but always confined within color-neutral hadrons. We can study this property through the static quark-antiquark potential $V(r)$, the ground state energy of the gluon field in the presence of an infinitely heavy $Q\bar{Q}$ pair at a fixed separation r. As $V(r)$ is an intrinsically non-perturbative quantity, it is computed numerically on the lattice using Monte Carlo methods [1, 2].

Lattice computations are performed in a finite volume, in most cases with periodic boundary conditions in all space-time directions. Typically, the volume is chosen large compared to all physical scales of the problem, and the remaining volume dependence is treated as a systematic error. In this thesis we instead ask what happens to the low-lying energy levels when we shorten one spatial direction until this condition is violated.

In a periodic lattice, the flux tube of the gluon field can connect the $Q\bar{Q}$ pair either directly with path length r or by wrapping around the shortened direction of extent l with path length $l - r$. So instead of a single string state, we get two competing low-lying states, which are degenerate at $r = \frac{l}{2}$. Whether and how these two states mix is the central question of this thesis. The answer depends on the center symmetry of the gauge group, which distinguishes the confined from the deconfined phase, as the shortened direction acts like an inverse temperature. We study this in SU(2) lattice Yang-Mills theory in 3+1 dimensions, using a variational basis built from the direct and the wrapped Wilson lines.

In chapter 2 we start with the theoretical framework, from Wilson and Polyakov loops over the center symmetry to the spectrum we expect in both phases. In chapter 3 we explain the lattice setup and the analysis methods, which we use to obtain the results presented in chapter 4. Finally, in chapter 5 we compare our results with the expected spectrum, draw conclusions and give an outlook for future work.

Chapter 2

Theoretical Framework

The following sections give a brief overview of the conventions used throughout, the concepts to calculate the energy eigenvalues E_n of the $Q\bar{Q}$ pair and the spectrum we can expect. For a comprehensive introduction to lattice quantum chromodynamics we refer to [2].

2.1. Conventions and Notation

We consider a four-dimensional Euclidean space-time lattice with lattice spacing a and periodic boundary conditions in all directions. The numbers of lattice points in the spatial and temporal directions are denoted by n_{s_x}, n_{s_y}, n_{s_z} and N_t, such that the lattice has the spatial extents $l_x = n_{s_x}a$, $l_y = n_{s_y}a$, $l_z = n_{s_z}a$ and the temporal extent $N_t a$. As we later shorten the extent l_z, we denote it by $l = l_z$. Gauge fields are represented by link variables $U_\mu(x)$, which are in our case elements of the SU(2) gauge group associated with the links connecting neighboring lattice sites. The temperature T of the system is related to the temporal extent of the lattice by $T = \frac{1}{N_t a}$. The dynamics of the gauge field is described by the Wilson gauge action:

$$S[U] = \beta \sum_P \left(1 - \frac{1}{2}\,\mathrm{Re}\,\mathrm{tr}\,U_P\right) \quad \text{with} \quad \beta = \frac{2N_C}{g_0^2} = \frac{4}{g_0^2} \tag{2.1.1}$$

where the sum runs over all plaquettes U_P, the smallest closed loops of four links on the lattice, N_C is the number of colors and g_0 is the bare gauge coupling. The inverse coupling β sets the strength of the gluon interaction. All traces of Wilson and Polyakov loops are normalized by $\frac{1}{N_C} = \frac{1}{2}$, which we suppress in the notation, so that they equal 1 for trivial links, while the trace in the action is not normalized.

2.2. Wilson Loops and the Static Potential

Wilson loops are gauge-invariant observables. They consist of two Wilson lines $S(\boldsymbol{m}, \boldsymbol{n}, n_t)$, $S(\boldsymbol{m}, \boldsymbol{n}, 0)$ and two temporal transporters $T(\boldsymbol{n}, n_t)$, $T(\boldsymbol{m}, n_t)$, which form a closed loop $\mathcal{L}$ in space-time. On the

lattice, the Wilson loop $W_{\mathcal{L}}$ is defined as the trace of the path-ordered product of link variables along this closed loop $\mathcal{L}$:

$$W_{\mathcal{L}}\,[U] = \mathrm{tr}\left[S(\boldsymbol{m},\boldsymbol{n},n_t)T^{\dagger}(\boldsymbol{n},n_t)S^{\dagger}(\boldsymbol{m},\boldsymbol{n},0)T(\boldsymbol{m},n_t)\right] = \mathrm{tr}\left[\prod_{(k,\mu)\in\,\mathcal{L}} U_{\mu}(k)\right] \tag{2.2.1}$$

$$\text{with}\quad S(\boldsymbol{m},\boldsymbol{n},n_t) = \prod_{(\boldsymbol{k},j)\in\mathcal{C}_{m,n}} U_j(\boldsymbol{k},n_t) \quad\text{and}\quad T(\boldsymbol{n},n_t) = \prod_{t=0}^{n_t-1} U_0(\boldsymbol{n},t) \tag{2.2.2}$$

In our case only planar Wilson loops are relevant, where the two spatial points $\boldsymbol{m}$ and $\boldsymbol{n}$ lie on a common coordinate axis and are connected by a straight path $\mathcal{C}_{m,n}$, and the loop has the temporal extent $t = n_t a$. For further details see section 3.3 of [2].

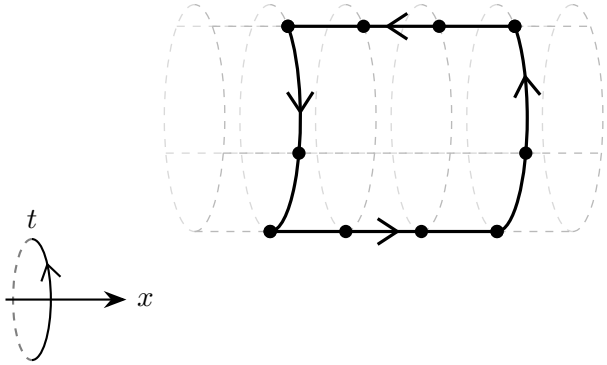


Figure 2.2.1: Planar Wilson loop in the x-t plane. The time direction is periodic, the loop lies on the front side of the lattice.

For a physical interpretation of the Wilson loop we use the spectral decomposition of a correlator on a lattice with infinite temporal extent:

$$\lim_{N_t\to\infty}\langle\mathcal{O}_1(t)\,\mathcal{O}_2^{\dagger}(0)\rangle = \sum_k \langle 0|\hat{\mathcal{O}}_1|k\rangle\langle k|\hat{\mathcal{O}}_2^{\dagger}|0\rangle\, e^{-E_k\,t} \tag{2.2.3}$$

Using (2.2.3) and temporal gauge fixing, where $T(\boldsymbol{n},n_t) = T(\boldsymbol{m},n_t) = \mathbb{1}$, we get for the expectation value of the Wilson loop:

$$\begin{aligned}\langle W_{\mathcal{L}}\rangle = \langle W_{\mathcal{L}}\rangle_{temp} &= \left\langle \mathrm{tr}\left[S(\boldsymbol{m},\boldsymbol{n},n_t)S^{\dagger}(\boldsymbol{m},\boldsymbol{n},0)\right]\right\rangle \\ &= \sum_k \langle 0|\hat{S}(\boldsymbol{m},\boldsymbol{n})_{ab}|k\rangle\langle k|\hat{S}^{\dagger}(\boldsymbol{m},\boldsymbol{n})_{ba}|0\rangle\, e^{-E_k\,t} \\ &\propto e^{-V(r)\,t}\left(1+\mathcal{O}(e^{-\Delta E\,t})\right)\end{aligned} \tag{2.2.4}$$

The states $|k\rangle$ with nonvanishing overlap with $\hat{S}^{\dagger}(\boldsymbol{m},\boldsymbol{n})|0\rangle$ describe a static $Q\bar{Q}$ pair at spatial separation $r = a|\boldsymbol{m}-\boldsymbol{n}|$. The corresponding lowest energy $E_0 = V(r)$ is the energy of the gluon field in the presence of this static $Q\bar{Q}$ pair, the static potential. Higher states contain gluonic excitations, whose contributions are exponentially suppressed by the energy difference $\Delta E = E_1 - E_0$ to the first excited state.

The static potential $V(r)$ can be parametrized by the Cornell potential [3]:

$$V(r) = A - \frac{\alpha_C}{r} + \sigma r \tag{2.2.5}$$

where A is a constant for the normalization of the energy, the second term is a Coulomb-like term with the coefficient α_C, which dominates at small separations, and the third term rises linearly with the string tension σ. This linearly rising term is the signature of confinement. It is physically interpreted as the self-interaction of the gluon field squeezing the field lines into a narrow flux tube between the static charges, whose energy grows with its length. Separating the $Q\bar{Q}$ pair would therefore require an infinite amount of energy, so that the static charges remain confined. In pure SU(2) gauge theory there are no dynamical quarks, so the flux tube cannot break by creating a light quark-antiquark pair and the potential keeps rising linearly.

2.3. Polyakov Loops and Center Symmetry

If we enlarge the temporal extent of a Wilson loop to the whole lattice $n_t \to N_t$, the temporal transporters close around the periodic time direction. A single such closed temporal line is the Polyakov loop

$$P(\boldsymbol{n}) = \mathrm{tr}\left[T(\boldsymbol{n}, N_t)\right] = \mathrm{tr}\left[\prod_{t=0}^{N_t-1} U_0(\boldsymbol{n}, t)\right] \tag{2.3.1}$$

which describes a single static quark propagating once around the periodic time direction. The correlator of two Polyakov loops with opposite orientation is related to the free energy $F_{Q\bar{Q}}(r)$ of a static $Q\bar{Q}$ pair at separation r [4]:

$$\langle P(\boldsymbol{n}) P^\dagger(\boldsymbol{m}) \rangle = e^{-\frac{F_{Q\bar{Q}}(r)}{T}} \tag{2.3.2}$$

For low temperatures, i.e. $N_t \to \infty$, the free energy reduces to the static potential and the correlator decays as $e^{-\frac{V(r)}{T}} = e^{-V(r)\,N_t a}$, like the Wilson loop $e^{-V(r)\,t}$ with $t = N_t a$.

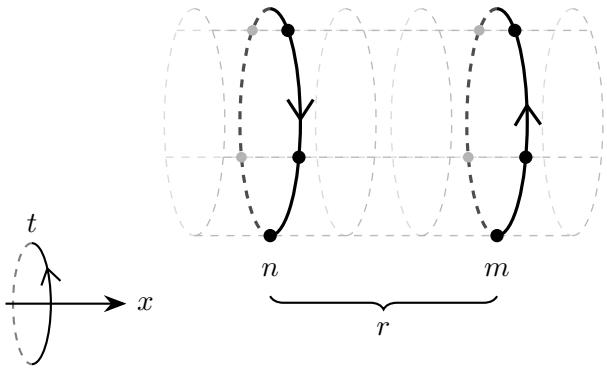


Figure 2.3.1: Two Polyakov loops $P(\boldsymbol{n})$ and $P^\dagger(\boldsymbol{m})$ separated by r. Due to the periodic boundary conditions in time direction, each loop closes around the back of the lattice.

For large distances r the correlator factorizes into the product of two single Polyakov loops:

$$\lim_{r\longrightarrow\infty}\langle P(\boldsymbol{n})P^\dagger(\boldsymbol{m})\rangle = \langle P(\boldsymbol{n})\rangle\langle P^\dagger(\boldsymbol{m})\rangle = |\langle P\rangle|^2 \quad \text{with} \quad P = \frac{1}{n_{s_x}n_{s_y}n_{s_z}}\sum_{\boldsymbol{n}} P(\boldsymbol{n}) \tag{2.3.3}$$

Using that for large separations the free energy of the pair is the sum of two isolated static quarks $F_{Q\bar{Q}}(r\to\infty) = 2F_Q$, we get

$$|\langle P\rangle| = e^{-\frac{F_Q}{T}} \tag{2.3.4}$$

So we may interpret the expectation value of the Polyakov loop as a measure for the probability of finding a single static quark in the system. If the free energy F_Q is infinite, we can never find a single static quark and $\langle P\rangle$ vanishes. This is exactly what we expect in the confined phase, while a non-vanishing $\langle P\rangle$ signals the deconfined phase. Which phase is realized depends on the temperature and the two phases are separated by the critical temperature T_c, which we discuss in section 2.3.2.

2.3.1. Center Transformations

Confinement is also related to a global symmetry of the Yang-Mills action, the center symmetry Z_N of the gauge group. For SU(2) the center group is $Z_2 = \{\mathbb{1}, -\mathbb{1}\}$, the set of elements that commute with all elements of the gauge group. A center transformation multiplies all temporal links on a fixed time slice t_0 by a center element $z \in Z_2$:

$$U_0(\boldsymbol{n}, t_0) \longrightarrow z\, U_0(\boldsymbol{n}, t_0) \quad \text{for all} \quad \boldsymbol{n} \tag{2.3.5}$$

The action is built from closed loops, which cross every time slice as often forward as backward. Since z commutes with all group elements, the factors z and $z^\dagger$ cancel with $z\,z^\dagger = \mathbb{1}$ and the action stays invariant. For the plaquette in the j-0 plane at t_0 this reads:

$$\begin{aligned} &\operatorname{tr}\left[U_j(\boldsymbol{n}, t_0)U_0(\boldsymbol{n}+\hat{\jmath}, t_0)U_j^\dagger(\boldsymbol{n}, t_0+1)U_0^\dagger(\boldsymbol{n}, t_0)\right] \\ \longrightarrow\ &\operatorname{tr}\left[U_j(\boldsymbol{n}, t_0)\, z\, U_0(\boldsymbol{n}+\hat{\jmath}, t_0)U_j^\dagger(\boldsymbol{n}, t_0+1)U_0^\dagger(\boldsymbol{n}, t_0)\, z^\dagger\right] \\ =\ &\operatorname{tr}\left[U_j(\boldsymbol{n}, t_0)U_0(\boldsymbol{n}+\hat{\jmath}, t_0)U_j^\dagger(\boldsymbol{n}, t_0+1)U_0^\dagger(\boldsymbol{n}, t_0)\right] \end{aligned} \tag{2.3.6}$$

2.3.2. The Polyakov Loop as an Order Parameter

Unlike the Wilson loop, the Polyakov loop is not invariant under center transformations. It winds once around the temporal direction and therefore crosses the time slice t_0 exactly once:

$$P(\boldsymbol{n}) \longrightarrow z\, P(\boldsymbol{n}) \tag{2.3.7}$$

If the center symmetry is unbroken, every configuration contributes with the same Boltzmann weight as its center-transformed configuration and the expectation value of the Polyakov loop vanishes:

$$\langle P\rangle = \frac{1}{2}\langle P + z\,P\rangle = \frac{1}{2}\,(1-1)\,\langle P\rangle = 0 \quad \text{for} \quad z = -\mathbb{1} \tag{2.3.8}$$

A non-vanishing $\langle P \rangle$ therefore signals the spontaneous breaking of the center symmetry.[1] Together with the free energy of a single static quark we get:

$$\text{confinement} \iff \langle P \rangle = 0 \iff F_Q \text{ infinite} \iff \text{unbroken } Z_2 \iff T < T_c \quad (2.3.9)$$

$$\text{deconfinement} \iff \langle P \rangle \neq 0 \iff F_Q \text{ finite} \iff \text{broken } Z_2 \iff T > T_c \quad (2.3.10)$$

To see why the broken phase is realized at high temperatures, we integrate out the spatial links in a strong coupling expansion. To leading order this gives an effective three-dimensional theory of the Polyakov loops [5, 6, 7]:

$$S_{\text{eff}} = -\lambda \sum_{\langle \boldsymbol{x}, \boldsymbol{y} \rangle} P(\boldsymbol{x})\, P(\boldsymbol{y}) \quad \text{with} \quad \lambda \propto u(\beta)^{N_t}, \quad u(\beta) = \frac{I_2(\beta)}{I_1(\beta)} < 1 \quad (2.3.11)$$

Like the Ising model, it is invariant under $P \to -P$. For small couplings λ the Polyakov loops are disordered and $\langle P \rangle = 0$, while above a critical coupling λ_c they align and $\langle P \rangle \neq 0$. Since $u < 1$, the coupling grows when N_t decreases, i.e. when the temperature $T = \frac{1}{N_t a}$ increases. So the center symmetry is broken above the critical temperature T_c defined by $\lambda(T_c) = \lambda_c$. Svetitsky and Yaffe [8] conjectured that the transition lies in the universality class of a three-dimensional spin model with the center symmetry of the gauge group. For SU(2) with Z_2 this is the Ising model, so that the transition is of second order.

2.4. The Static $Q\bar{Q}$ Pair in a Periodic Volume

From (2.2.4) we know that the potential $V(r)$ of a static $Q\bar{Q}$ pair at a fixed separation r can be calculated from the expectation value of a Wilson loop. On a lattice with periodic boundary conditions the two static charges can be connected in two ways, either directly with path length r or by wrapping around the lattice with path length $l - r$, where l is the extent in the direction of the separation. Therefore we have to modify our Wilson loops and include the wrapped Wilson line.

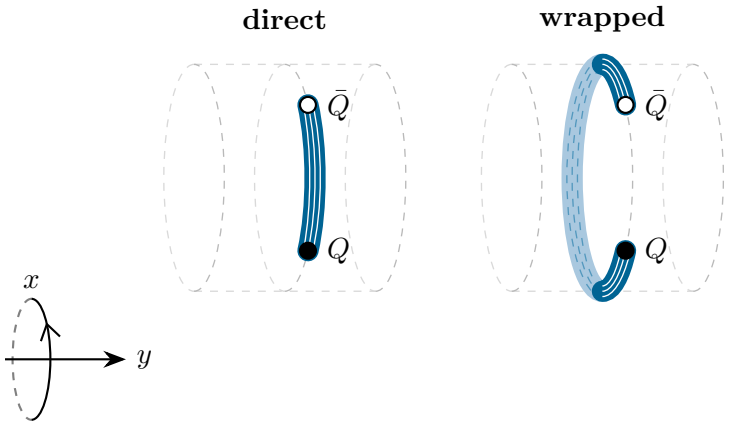


Figure 2.4.1: Physical picture of the static $Q\bar{Q}$ pair in a periodic volume. The quark and antiquark can be connected by a flux tube either directly or by wrapping around the periodic spatial direction.

[1] Strictly, a spontaneous symmetry breaking only occurs in infinite volume, so that on a finite lattice $\langle |P| \rangle$ is the appropriate order parameter. This more detailed treatment is left for future work (see chapter 5).

2.4.1. Direct and Wrapped Wilson Lines

The Wilson loop (2.2.1) contains the two Wilson lines $S(\boldsymbol{m}, \boldsymbol{n}, n_t)$ and $S(\boldsymbol{m}, \boldsymbol{n}, 0)$, which connect the two static charges at the times t and 0. As we have two possible ways to connect the charges, we consider two different Wilson lines. We denote by $\mathcal{O}_1(t) = S(\boldsymbol{m}, \boldsymbol{n}, n_t)_{\text{direct}}$ and $\mathcal{O}_1(0) = S(\boldsymbol{m}, \boldsymbol{n}, 0)_{\text{direct}}$ the direct Wilson lines with path length $r = a|\boldsymbol{m} - \boldsymbol{n}|$, and by $\mathcal{O}_2(t) = S(\boldsymbol{m}, \boldsymbol{n}, n_t)_{\text{wrapped}}$ and $\mathcal{O}_2(0) = S(\boldsymbol{m}, \boldsymbol{n}, 0)_{\text{wrapped}}$ the wrapped Wilson lines with path length $l - r$. Here $\boldsymbol{m} - \boldsymbol{n}$ points along a lattice axis and l denotes the extent of the lattice in that direction, which is the shortened extent for separations along z. Together with the temporal transporters they form a variational basis, from which we construct the correlation matrix $C_{ij}(t)$.

2.4.2. Correlation Matrix

Since $\mathcal{O}_1$ and $\mathcal{O}_2$ share the endpoints $\boldsymbol{m}$ and $\boldsymbol{n}$, the same temporal transporters close all four combinations of Wilson lines into loops:

$$\begin{aligned} C_{ij}(t) &= \Big\langle \operatorname{tr}\Big[\mathcal{O}_i(t)\, T^\dagger(\boldsymbol{n}, n_t)\, \mathcal{O}_j^\dagger(0)\, T(\boldsymbol{m}, n_t)\Big]\Big\rangle \\ &= \begin{pmatrix} \Big\langle \operatorname{tr}\Big[\mathcal{O}_1(t)\, T^\dagger(\boldsymbol{n}, n_t)\, \mathcal{O}_1^\dagger(0)\, T(\boldsymbol{m}, n_t)\Big]\Big\rangle & \Big\langle \operatorname{tr}\Big[\mathcal{O}_1(t)\, T^\dagger(\boldsymbol{n}, n_t)\, \mathcal{O}_2^\dagger(0)\, T(\boldsymbol{m}, n_t)\Big]\Big\rangle \\ \Big\langle \operatorname{tr}\Big[\mathcal{O}_2(t)\, T^\dagger(\boldsymbol{n}, n_t)\, \mathcal{O}_1^\dagger(0)\, T(\boldsymbol{m}, n_t)\Big]\Big\rangle & \Big\langle \operatorname{tr}\Big[\mathcal{O}_2(t)\, T^\dagger(\boldsymbol{n}, n_t)\, \mathcal{O}_2^\dagger(0)\, T(\boldsymbol{m}, n_t)\Big]\Big\rangle \end{pmatrix} \end{aligned} \tag{2.4.1}$$

where the product of link variables is understood as path ordered along the closed loop and the trace runs over color indices. The diagonal elements $C_{11}(t)$ and $C_{22}(t)$ are the direct and the wrapped Wilson loop, while the off-diagonal elements $C_{12}(t)$ and $C_{21}(t)$ are the cross-correlations between the direct and the wrapped Wilson line. The correlation matrix satisfies $C_{ij}(t) = C_{ji}^*(t)$ and since all traces of SU(2) matrices are real, $C_{ij}(t)$ is a real symmetric matrix.

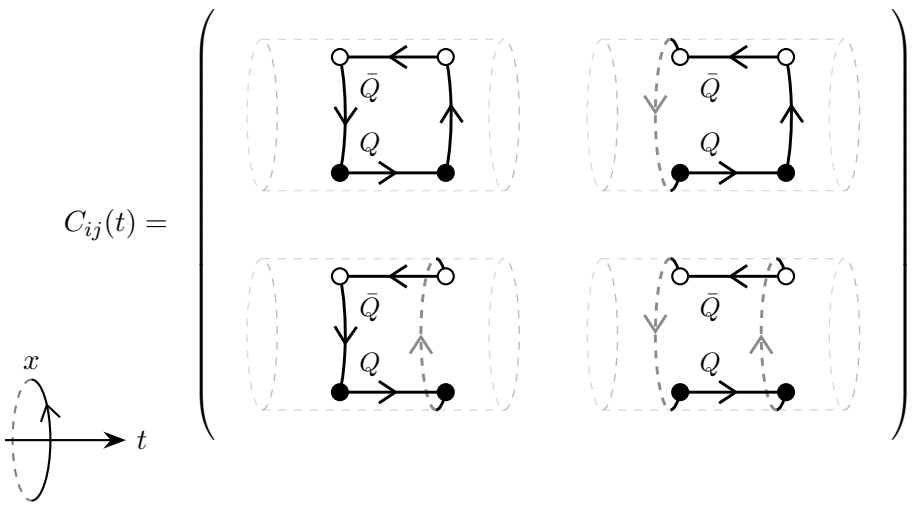


Figure 2.4.2: Visual representation of the correlation matrix with direct ($\mathcal{O}_1$) and wrapped ($\mathcal{O}_2$) Wilson lines in a volume that is periodic in the spatial direction x. The diagonal elements are the direct and the wrapped Wilson loop, the off-diagonal elements are one-sided wrapped Wilson loops describing transition amplitudes.

The correlation matrix can also be used to extract the energy spectrum of the system by a spectral decomposition of its elements. We work in temporal gauge, so that the temporal transporters become

trivial, $T(\boldsymbol{n}, n_t) = T(\boldsymbol{m}, n_t) = \mathbb{1}$, and the Euclidean time evolution is generated by the Hamiltonian $\hat{H}$ of the transfer matrix $\hat{\mathcal{T}} = e^{-a\hat{H}}$:

$$\hat{\mathcal{O}}_i(t) = e^{\hat{H}t}\,\hat{\mathcal{O}}_i\,e^{-\hat{H}t} \tag{2.4.2}$$

For a lattice with infinite temporal extent the expectation value becomes a vacuum expectation value and we insert a complete set of energy eigenstates $|n\rangle$ between the operators:

$$\begin{aligned}\lim_{N_t\to\infty} C_{ij}(t)_{temp} &= \left\langle \hat{\mathcal{O}}_i(t)\,\hat{\mathcal{O}}_j^\dagger(0)\right\rangle_\Omega = \left\langle \Omega \,\middle|\, e^{\hat{H}t}\,\hat{\mathcal{O}}_i\,e^{-\hat{H}t}\,\hat{\mathcal{O}}_j^\dagger \,\middle|\, \Omega\right\rangle \\ = \sum_{n=0}^{\infty} \left\langle \Omega \,\middle|\, \hat{\mathcal{O}}_i \,\middle|\, n\right\rangle \left\langle n \,\middle|\, e^{-\hat{H}t}\,\hat{\mathcal{O}}_j^\dagger \,\middle|\, \Omega\right\rangle e^{E_\Omega t} &= \sum_{n=0}^{\infty} \left\langle \Omega \,\middle|\, \hat{\mathcal{O}}_i \,\middle|\, n\right\rangle \left\langle n \,\middle|\, \hat{\mathcal{O}}_j^\dagger \,\middle|\, \Omega\right\rangle e^{-(E_n - E_\Omega)t} \\ &= \sum_{n=0}^{\infty} c_i^{(n)}\, c_j^{*(n)}\, e^{-E_n t}\end{aligned} \tag{2.4.3}$$

Here $|n\rangle$ are the energy eigenstates of the gluon field in the presence of the static $Q\bar{Q}$ pair, $|\Omega\rangle$ is the vacuum and E_n are the corresponding energies, where we set $E_\Omega = 0$, as only energy differences are relevant.

$$c_i^{(n)} = \left\langle \Omega \,\middle|\, \hat{\mathcal{O}}_i \,\middle|\, n\right\rangle \quad \text{and} \quad c_j^{*(n)} = \left\langle n \,\middle|\, \hat{\mathcal{O}}_j^\dagger \,\middle|\, \Omega\right\rangle \tag{2.4.4}$$

are the overlaps of the trial states $\hat{\mathcal{O}}_i^\dagger|\Omega\rangle$ with the energy eigenstates. Only for the diagonal elements does this reduce to a modulus squared $C_{ii}(t) = \sum_{n=0}^{\infty} \left|c_i^{(n)}\right|^2 e^{-E_n t}$, whereas for $i \neq j$ the two overlaps belong to different operators and $C_{ij}(t)$ does not have to be positive.

2.4.3. Confinement Constraints on the Off-Diagonal Elements

As shown in (2.3.7), the Polyakov loop transforms under center transformations, because it crosses every time slice exactly once. As the Wilson action treats all four directions equally, we can interchange the roles of the temporal and the shortened spatial direction. Interpreting the shortened direction as a Euclidean time direction, our lattice describes a system at the temperature $T = \frac{1}{l}$, while the actual temperature $\frac{1}{N_t a}$ remains small. In the following T denotes this temperature of the shortened direction. Shortening l therefore acts like raising the temperature, and we expect deconfinement along the shortened direction for $l < \frac{1}{T_c}$. The center transformation now multiplies all links pointing in the shortened direction on one slice by $z \in Z_2$. The off-diagonal elements of the correlation matrix wind once around the shortened direction, as the path of $\mathcal{O}_1\mathcal{O}_2^\dagger$ has the length $r + (l - r) = l$. So they cross every such slice exactly once and transform as

$$C_{ij}(t) \longrightarrow z\,C_{ij}(t) \quad \text{for} \quad i \neq j \tag{2.4.5}$$

while the diagonal elements stay invariant. Analogous to the Polyakov loop, the off-diagonal elements vanish if the center symmetry is unbroken:

$$\langle C_{ij}(t)\rangle = \frac{1}{2}\left\langle C_{ij}(t) + z\,C_{ij}(t)\right\rangle = \frac{1}{2}\,(1-1)\left\langle C_{ij}(t)\right\rangle = 0 \quad \text{for} \quad i \neq j,\ z = -\mathbb{1} \tag{2.4.6}$$

Linking this to (2.3.9) and (2.3.10), the off-diagonal elements vanish in the confined phase and are non-zero in the deconfined phase:

$$\text{confinement} \iff \text{unbroken } Z_2 \iff \langle C_{ij}(t)\rangle = 0 \quad \text{for} \quad i \neq j \iff T < T_c \tag{2.4.7}$$

$$\text{deconfinement} \iff \text{broken } Z_2 \iff \langle C_{ij}(t)\rangle \neq 0 \quad \text{for} \quad i \neq j \iff T > T_c \tag{2.4.8}$$

For $t = 0$ the off-diagonal elements reduce to the Polyakov loop around the shortened direction, so that they directly measure the order parameter of the center symmetry.

2.5. Expected Spectrum

According to (2.4.3) the correlation matrix is a sum of exponentials $e^{-E_n t}$ and therefore contains the energy levels E_n of the static $Q\bar{Q}$ pair. In the following we discuss which levels we expect in the confined and in the deconfined phase.

2.5.1. Sharp Level Crossing in Confinement

Let us first consider the easier case of confinement. As the off-diagonal elements vanish, the correlation matrix $C_{ij}(t)$ is diagonal and its two diagonal elements can be treated independently. The reason for this is that the direct and the wrapped Wilson line behave differently under center transformations, as only the product $\mathcal{O}_1\mathcal{O}_2^\dagger$ winds around the shortened direction. As long as the center symmetry is unbroken, the time evolution can therefore not turn a direct into a wrapped state and the two states do not mix. The energy levels are simply the energies of the direct $V(r)$ and the wrapped string $V(l-r)$. The ground state is always given by the shorter of the two strings, so the two levels meet at $r = \frac{l}{2}$, where both strings have the same length. As the two states do not mix, nothing prevents the levels from crossing and we expect a sharp level crossing at $r = \frac{l}{2}$. The ground state $V_0(r)$ follows the direct string for $r < \frac{l}{2}$ and the wrapped string for $r > \frac{l}{2}$, the first excited state $V_1(r)$ vice versa.

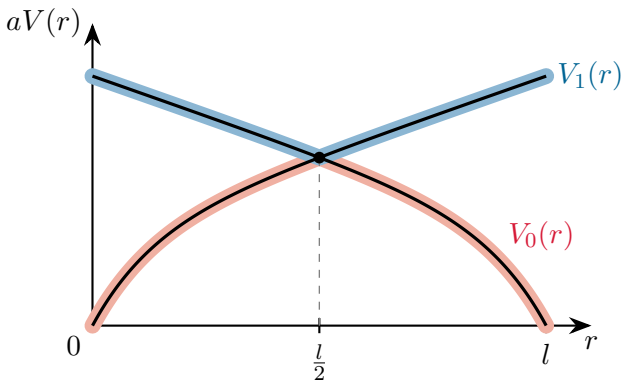


Figure 2.5.1: Sketch of the expected energy spectrum in the confined phase. The energies of the direct and the wrapped string cross sharply at $r = \frac{l}{2}$.

2.5.2. Sector Selection and Avoided Level Crossing

In the deconfined phase the off-diagonal elements have a non-vanishing expectation value and the correlation matrix is no longer diagonal, so that the energies have to be extracted by solving a generalized eigenvalue problem (see chapter 3). The energy eigenstates $|n\rangle$ are now linear combinations of the direct and the wrapped state, i.e. the two states mix. According to the non-crossing rule of von Neumann and Wigner [9], the levels of two states that can mix do not cross, so we expect an avoided level crossing at $r = \frac{l}{2}$. This can be described by an effective two-level system of the direct and the wrapped state with the mixing strength δ:

$$H_{\text{eff}} = \begin{pmatrix} V(r) & \delta \\ \delta & V(l-r) \end{pmatrix} \quad \Longrightarrow \quad V_{0,1}(r) = \frac{V(r) + V(l-r)}{2} \mp \sqrt{\frac{\left(V(r) - V(l-r)\right)^2}{4} + \delta^2} \tag{2.5.1}$$

Far away from $r = \frac{l}{2}$ the levels approach the unmixed energies $V(r)$ and $V(l-r)$, while at $r = \frac{l}{2}$ they are separated by the level splitting $\Delta E\left(\frac{l}{2}\right) = 2\delta$. In the confined phase $\delta = 0$ and the sharp level crossing is recovered. The same mixing of two string-type states with an avoided level crossing is known from string breaking, where the string state mixes with a state of two static-light mesons [10, 11]. The sign of the off-diagonal elements depends on which of the two Z_2 sectors the system selects, as a center transformation flips the relative sign of $\mathcal{O}_1$ and $\mathcal{O}_2$. This corresponds to the change of basis $\mathcal{O}_2 \to -\mathcal{O}_2$, which leaves the energies unchanged, so both sectors yield the same spectrum. As the center transformation along the shortened direction is an exact symmetry, averaging over both sectors would again give vanishing off-diagonal elements and a sharp level crossing. The avoided level crossing is therefore a property within one sector, which is selected spontaneously in the deconfined phase.

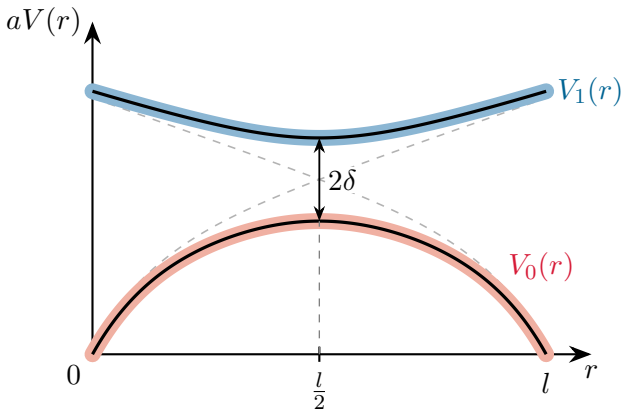


Figure 2.5.2: Sketch of the expected energy spectrum in the deconfined phase. The mixing of the direct and the wrapped states lifts the degeneracy at $r = \frac{l}{2}$ and leads to an avoided level crossing. Dashed lines show the unmixed energies of the sharp level crossing.

2.5.3. Further Excited States at Small Separations

A glueball is a bound state consisting only of gluons, classified by the quantum numbers J^{PC} of total angular momentum J, parity P and charge conjugation C. The lightest glueball 0^{++} [12, 13] carries the quantum numbers of the vacuum and can therefore be created from it without violating any

conservation law. So the wrapped string is only the first excited level as long as $V(l-r) - V(r) < m_G$. For small separations r and a large extent l the wrapped string energy $V(l-r)$ exceeds the threshold $V(r) + m_G$. The lowest excited level is then no longer a string state but a two-particle state of the ground-state $Q\bar{Q}$ pair and a glueball, so we expect $V_1(r) \to V_0(r) + m_G$ at small separations. In a volume with a short extent, states of flux loops winding around it can be lighter than the glueball [14]. In addition the direct Wilson line overlaps with an excited flux tube with the same quantum numbers as the ground state [15]. Since neither $\mathcal{O}_1$ nor $\mathcal{O}_2$ is built to create these states, they have only a small overlap with our operator basis.

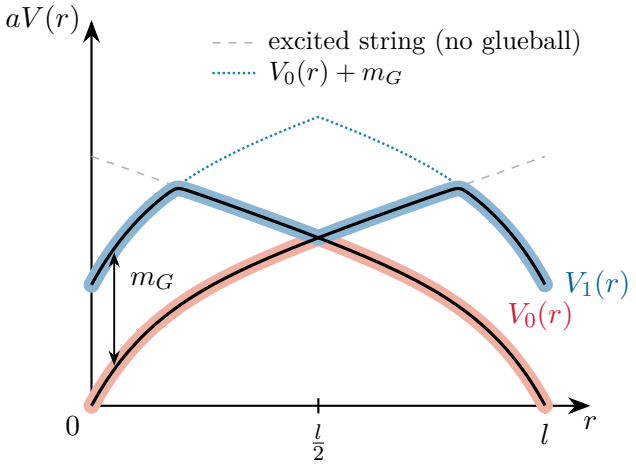


Figure 2.5.3: Sketch of the expected energy spectrum in the confined phase including the glueball threshold. The direct and the wrapped string cross sharply at $r = \frac{l}{2}$. Towards small separations and by periodicity towards $r \to l$, the excited string state (dashed) rises above the two-particle state of the $Q\bar{Q}$ ground state and a glueball (dotted), so that $V_1(r) \to V_0(r) + m_G$.

Chapter 3

Simulation and Analysis Methods

To test the expected spectrum, we perform Monte Carlo simulations on the lattice and analyze the generated data. We shorten only the spatial extent l and keep all other extents large, including the temporal extent, so that the actual temperature $T = \frac{1}{N_t a}$ stays far below the critical temperature. As discussed in section 2.4.3, the shortened direction then acts like a system at the temperature $T = \frac{1}{l}$. With the critical couplings $\beta_c(N_t = 4) \approx 2.30$, $\beta_c(N_t = 6) \approx 2.43$ and $\beta_c(N_t = 8) \approx 2.51$ [16], at $\beta = 2.40$ the extent $l = 4a$ lies in the deconfined phase, whereas $l = 6a$ lies just below and $l = 8a$ below the critical temperature. The following sections give a brief overview of the methods we used to generate the gauge fields, solve the generalized eigenvalue problem, perform the statistical analysis and set the scale of our results.

3.1. Gauge Field Generation and Smearing

Before we can calculate any observables, we have to generate the underlying gauge field configurations on the lattice. They are generated using the heatbath algorithm of Creutz [1], a Markov chain Monte Carlo method that samples gauge field configurations according to the Boltzmann weight $e^{-S[U]}$. The algorithm updates a single link by drawing it from its conditional distribution given the surrounding staples, while all other links are held fixed. For SU(2) this can be done exactly, since the sum of the staples is itself proportional to an SU(2) matrix. Systematically updating all gauge links in that way is referred to as a sweep through the lattice. After a sufficient number of sweeps the Markov chain has reached equilibrium, called the thermalized state.

The heatbath algorithm can be started either from a hot start, a completely random gauge field configuration, or from a cold start, where all gauge links are set to the identity. Whether equilibrium has been reached is checked by monitoring the average plaquette and the Polyakov loop along the shortened direction, which we measure as the off-diagonal element $C_{12}(t = 0)$ of the correlation matrix. For $l = 6a$ we performed both a hot and a cold start, which have to fluctuate around the same values. The thermalization of the three lattice setups can be seen in appendix A. We discard the first $N_{therm} = 300$ sweeps and keep $N_{meas} = 111$ configurations.

Since each configuration is generated from the previous one, successive configurations are correlated and the measurements performed on them are not statistically independent. To reduce this autocor-

relation we perform $N_{save} = 30$ sweeps between two measurements, which is large compared to the autocorrelation time of the plaquette of a few sweeps. Close to the critical temperature, i.e. for $l = 6a$, the Polyakov loop along the shortened direction decorrelates considerably slower.

To reduce the noise in the measurements, we apply smearing to the gauge fields, which smooths out short-distance fluctuations and enhances the signal of long-distance physics. The temporal links, which form the propagators of the static quarks, are replaced by HYP2 links with $(\alpha_1, \alpha_2, \alpha_3) = (1.0, 1.0, 0.5)$ [17, 18]. This reduces the self-energy of the static quarks and thereby the noise at large t, but shifts all energies E_n by the same r-independent constant, which cancels in energy differences and in the fit parameters α_C and σ. The spatial links are APE smeared [19], where each spatial link is replaced by itself plus the sum of its four spatial staples:

$$U_k^{(n+1)}(x) = P_{\mathrm{SU}(2)} \left[U_k^{(n)}(x) + \alpha \sum_{\text{staples}} \Sigma_k^{(n)}(x) \right] \quad \text{for} \quad k = 1, 2, 3 \tag{3.1.1}$$

where all links of one iteration are built from the previous field $U^{(n)}$. Since any real linear combination of SU(2) matrices is again proportional to an SU(2) matrix, the projection $P_{\mathrm{SU}(2)}$ reduces to a normalization by $\sqrt{\det}$. Both operators $\mathcal{O}_1$ and $\mathcal{O}_2$ are built from the same smeared links and differ only in their geometry. APE smearing modifies only the overlaps $c_i^{(n)}$ of the operators with the energy eigenstates, which improves the signal at small t but must not change the extracted energies E_n within statistical errors. We use $\alpha = 0.5$ and $i_{smear} = 5$ smearing iterations, chosen such that the effective energy plateaus set in as early as possible.

β	N_t, n_{s_x} and n_{s_y}	n_{s_z}	N_{therm}	N_{save}	N_{total}	N_{meas}	α	i_{smear}
2.40	24	8	300	30	3600	111	0.5	5
2.40	24	6	300	30	3600	111	0.5	5
2.40	24	4	300	30	3600	111	0.5	5

Table 3.1.1: Parameters of the three lattice setups. All runs use a cold start, for $n_{s_z} = 6$ an additional hot start was performed. The temporal links are HYP2 smeared in all runs.

3.2. Generalized Eigenvalue Problem

On every configuration we compute the correlation matrix $C_{ij}(t)$ from section 2.4.2 for all separations r and times t, averaged over all lattice sites. Wilson loops along x and y probe the long directions, while Wilson loops along z probe the shortened direction. As $C_{12}(t)$ and $C_{21}(t)$ agree only up to statistical fluctuations, we symmetrize the averaged matrix $C \to \frac{1}{2}(C + C^T)$. The energy spectrum is then extracted by solving the generalized eigenvalue problem, short GEVP [20, 21]:

$$C(t)\, v_n = \lambda_n\, C(t_0)\, v_n \tag{3.2.1}$$

with the eigenvalues ordered as $\lambda_0 \geq \lambda_1$. We solve the GEVP once at $t_0 = 2a$ and $t = 3a$, where the signal is still precise and $C(t_0)$ is well conditioned. The eigenvectors give the linear combinations of

$\mathcal{O}_1$ and $\mathcal{O}_2$ with maximal overlap onto the corresponding eigenstate, so that the projected correlators $C_n(t) = v_n^T\, C(t)\, v_n$ are dominated by a single state already at small t. From these we define the effective energies

$$aE_n^{\text{eff}}(t) = \ln\left(\frac{C_n(t-a)}{C_n(t)}\right) \quad \text{with} \quad E_n^{\text{eff}}(t) \to E_n \quad \text{for} \quad t \to \infty \tag{3.2.2}$$

and read off E_n from a constant fit to the plateau region $3a \leq t \leq 20a$, i.e. a weighted average with the inverse squared jackknife errors as weights. Examples of these plateaus are shown in appendix B. Repeating this for every separation r gives the ground state $V_0(r) = E_0$ and the first excited state $V_1(r) = E_1$. From these we determine the level splitting $\Delta E\left(\frac{l}{2}\right) = V_1\left(\frac{l}{2}\right) - V_0\left(\frac{l}{2}\right)$ in the shortened direction. In the long directions the center symmetry is unbroken, so the off-diagonal elements vanish and the GEVP reduces to two independent effective masses.

3.3. Statistical Analysis

Every numerical analysis is contaminated by uncertainties, which are a combination of systematic and statistical errors. The statistical errors are due to the stochastic nature of the sampling. They are not easily obtained by linear error propagation, because the GEVP and the effective energies are non-linear functions of correlated Monte Carlo averages. We therefore use the jackknife method, in which $N = N_{meas}$ reduced samples are formed by omitting one measurement at a time. Denoting by $\bar{\theta}_{(i)}$ the estimator evaluated on the sample with the i-th measurement removed and by $\bar{\theta}$ the estimator on the full sample, the jackknife error is

$$\sigma^2_{\text{jack}} = \frac{N-1}{N}\sum_{i=1}^{N}\left(\bar{\theta}_{(i)} - \bar{\theta}\right)^2 \tag{3.3.1}$$

where the prefactor $(N-1)$ compensates the reduced fluctuation of the strongly overlapping samples. The analysis chain, from the correlation matrix over the solution of the GEVP to the plateau fit, is carried out separately on every jackknife sample, where the eigenvalues are ordered by magnitude. Only in this way do the resulting errors propagate consistently through the non-linear steps. We do not apply binning, as the autocorrelation of the plaquette is small compared to the $N_{save} = 30$ sweeps between two measurements. Close to the critical temperature, i.e. for $l = 6a$, the Polyakov loop along the shortened direction decorrelates considerably slower, so that the errors of the off-diagonal elements for $l = 6a$ are likely underestimated.

The systematic errors are due to the finite lattice spacing, the truncation of the operator basis, the choice of the plateau range in t and the convention entering the scale setting. The plateau range is the dominant source among them. Starting the plateau fit at $t = 4a$ instead of $3a$ shifts, for example $V_0(r = 8a)$ by about 4σ, which shows that excited states are not fully suppressed at $t = 3a$ for larger separations. In the long directions this biases the potential upwards at large r, its slope for $r \gtrsim 6a$ decreases from about 0.084 to 0.078 per lattice spacing when starting the plateau at $t = 4a$. Both values lie about 10 to 18 % above the string tension $a^2\sigma \approx 0.071$ [22]. As the weights of the plateau fit are dominated by the early timeslices and correlations between timeslices are neglected, we do not

quote a χ^2 for the plateau fits. The upper end $t = 20a$ lies close to $N_t a = 24a$, where contributions propagating around the periodic time direction appear, but reducing it to $t = 15a$ changes the level splittings by less than 0.001. For $r \leq 4a$, which is all we need for the level splittings at $r = \frac{l}{2}$, the energies change by at most 0.01 and the splittings for $l = 6a$ and $8a$ by less than 0.001. In addition, for $r \leq 2a$ the HYP smeared temporal links of the two static quarks are built from partly the same links, which lowers the energies at these separations. This is visible as a violation of the concavity of the potential [23] between $r = a$ and $3a$, which does not depend on the plateau range, and as the small value $aV_0(a) \approx 0.059$. The finite spatial volume is not treated as a systematic error here, since the dependence of the static potential on the shortened extent is the subject of this thesis.

3.4. Scale Setting

Pure SU(2) gauge theory contains no experimental input, so there is no intrinsic physical scale. To express our results in physical units, we use the Sommer parameter r_0 [24], which is defined implicitly by the force $F(r) = V'(r)$ between a static quark-antiquark pair through the dimensionless condition:

$$r^2 F(r)\Big|_{r=r_0} = 1.65 \tag{3.4.1}$$

Assigning a value to r_0 is a convention taken over from QCD phenomenology and all results quoted in physical units are to be understood relative to this choice. Following Philipsen and Wagner [25], who determined the static potential for SU(2) using $r_0 = 0.46$ fm, we use a lattice spacing of $a = 0.102$ fm at $\beta = 2.40$.

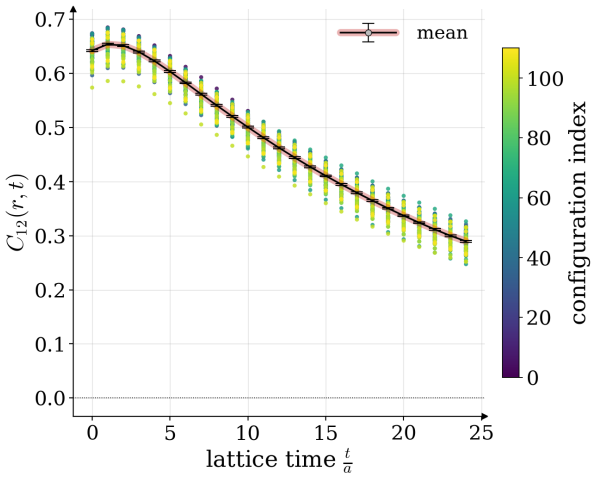
Chapter 4

Numerical Results

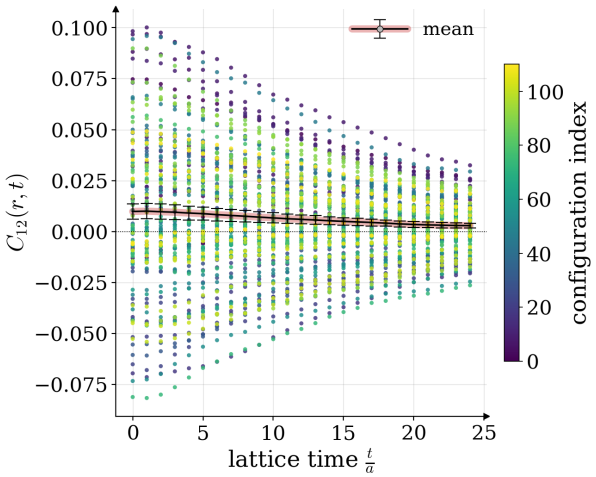
In this chapter we present the energy levels $V_0(r)$ and $V_1(r)$ obtained with the methods of chapter 3 and compare them with the expected spectrum of section 2.5. We first check whether the off-diagonal elements of the correlation matrix behave as predicted by the center symmetry. Then we discuss the spectrum along the shortened direction for $l = 8a$, $6a$ and $4a$, the level splitting at $r = \frac{l}{2}$ and finally the spectrum along a long direction. All energies are given in lattice units. With $a = 0.102$ fm [25] the three extents correspond to the temperatures $T = \frac{1}{l} \approx 242$ MeV, 322 MeV and 484 MeV.

4.1. Off-Diagonal Elements and Center Symmetry

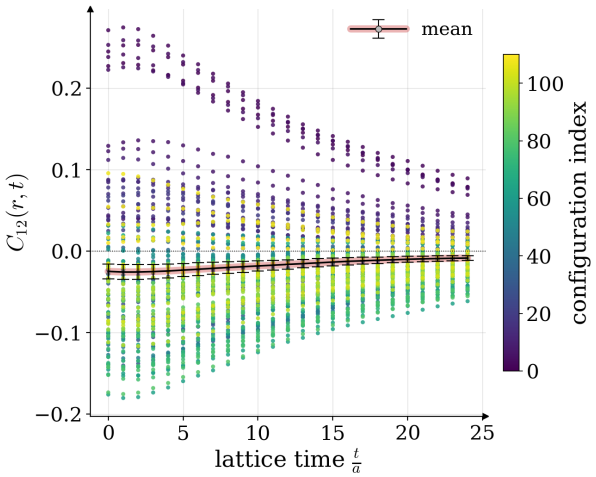
According to section 2.4.3, the off-diagonal elements of the correlation matrix vanish in the confined phase and are non-zero in the deconfined phase. Figure 4.1.1 shows $C_{12}(t)$ at $r = a$ on all configurations together with its mean. For $t = 0$ it reduces to the Polyakov loop around the shortened direction, which is independent of r. For $l = 4a$ the off-diagonal element is large $C_{12}(0) \approx 0.64$, and positive on all configurations. As it is built from APE smeared links, this value is larger than the unsmeared Polyakov loop and cannot be compared directly with literature values. So the center symmetry is broken and the system remains in the positive sector, which is selected by the cold start, during the whole simulation. For $l = 8a$ it fluctuates around zero with a mean of about 0.01, as expected in the confined phase. For $l = 6a$ both starts show long excursions into the two sectors (see appendix A). The cold start begins at $C_{12}(0) \approx 0.25$ and stays around -0.1 for most of the later measurements, while the hot start remains at positive values up to about 0.25 from configuration 30 to 74. This gives a mean of -0.03 for the cold start and $+0.06$ for the hot start. This slow decorrelation reflects that $l = 6a$ lies close to the critical temperature. The off-diagonal elements therefore confirm that $l = 4a$ is deconfined and $l = 8a$ confined, while the long excursions for $l = 6a$ show that it lies close to the transition.



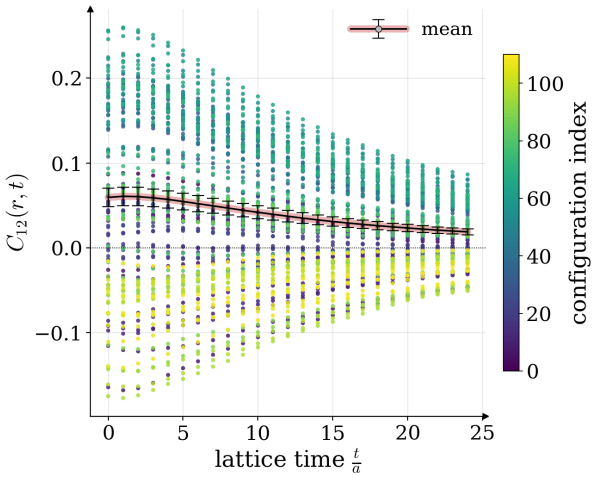
(a) $l = 4a$, cold start



(b) $l = 8a$, cold start



(c) $l = 6a$, cold start



(d) $l = 6a$, hot start

Figure 4.1.1: Off-diagonal element $C_{12}(t)$ at $r = a$ along the shortened direction on all 111 configurations and its mean. For $t = 0$ it is the Polyakov loop around the shortened direction.

4.2. Energy Spectrum along the Shortened Direction

The following figures show the ground state $V_0(r)$ and the first excited state $V_1(r)$ for $0 \leq r \leq l$. Due to the periodicity the spectrum is symmetric around $r = \frac{l}{2}$. At $r = 0$ and $r = l$ the direct Wilson line has no spatial extent, so that $V_0 = 0$ holds by construction and does not contain the self-energy of the static quarks. For comparison we show the unmixed energies $V(r)$ and $V(l - r)$ as dashed lines, where $V(r)$ is the ground state measured along the long direction x of the same run. So the figures can be compared directly with the sketches of section 2.5.

4.2.1. Confined Extent $l = 8a$

Figure 4.2.1 shows the sharp level crossing expected in the confined phase. For $r < \frac{l}{2}$ the ground state follows the direct string and agrees with the potential of the long directions, e.g. $aV_0(2a) = 0.134$ compared to 0.136. The first excited state follows the wrapped string $V(l - r)$, which lies only slightly above the data at small r. At $r = 4a$ both levels meet with $aV_0 = 0.326(3)$ and $aV_1 = 0.335(3)$. As the eigenvalues are ordered, $\Delta E \geq 0$ holds on every jackknife sample, so that statistical fluctuations

always lead to a small positive splitting for degenerate levels. The remaining splitting $a\Delta E = 0.009(4)$ is of this size and therefore consistent with a sharp level crossing.

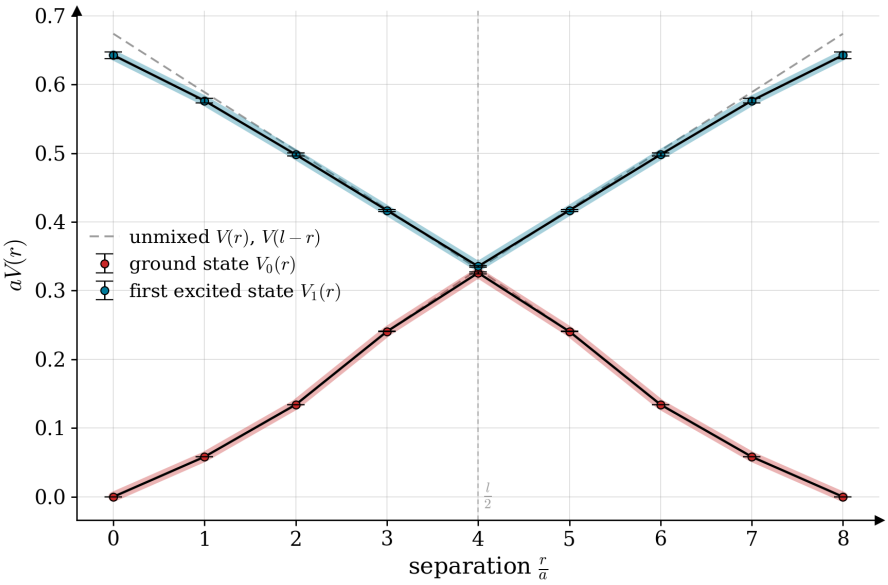
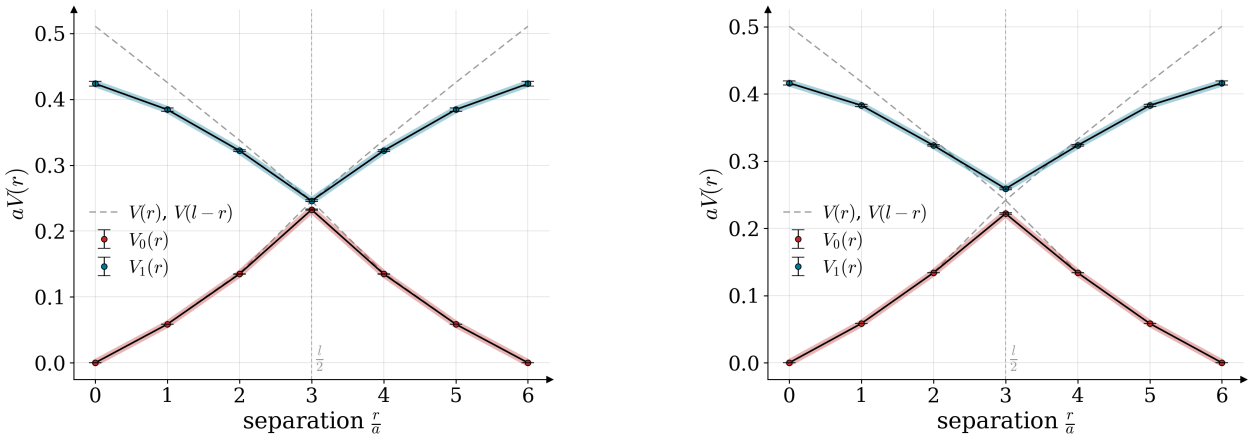


Figure 4.2.1: Ground state $V_0(r)$ and first excited state $V_1(r)$ along the shortened direction for $l = 8a$ (cold start). The dashed lines are the unmixed energies $V(r)$ and $V(l-r)$ of the long direction. The levels cross sharply at $r = \frac{l}{2}$.

4.2.2. Near-Critical Extent $l = 6a$

For $l = 6a$ the spectrum in figure 4.2.2 still shows a level crossing at $r = 3a$ close to the unmixed energies, but the splitting depends on the start. At small r the first excited state lies below the wrapped string of the long direction, e.g. $aV_1(a) = 0.384(5)$ for the cold start. This is expected close to the critical temperature, where the energy of a string winding around the shortened direction decreases. For the cold start we find $a\Delta E = 0.013(6)$, for the hot start $a\Delta E = 0.037(7)$. As both runs describe the same physics, the two values should agree, but they differ by about 2.5 standard deviations. This is consistent with the Monte Carlo histories of section 4.1. The hot start spends a long stretch in one sector with $C_{12}(0) \approx 0.2$, where the off-diagonal elements are sizable and the direct and the wrapped state mix, while the cold start mostly stays at $|C_{12}(0)| \approx 0.1$. So the statistical errors for $l = 6a$ are underestimated, since the Polyakov loop decorrelates only slowly close to the critical temperature and we do not apply binning. So for $l = 6a$ we can only conclude that the splitting is small, but not whether it vanishes.



(a) cold start

(b) hot start

Figure 4.2.2: Ground state $V_0(r)$ and first excited state $V_1(r)$ along the shortened direction for $l = 6a$. The dashed lines are the unmixed energies $V(r)$ and $V(l-r)$ of the long direction.

4.2.3. Deconfined Extent $l = 4a$

For $l = 4a$ figure 4.2.3 shows a clear avoided level crossing. As discussed in section 2.5, this result is obtained within one sector, as the system does not tunnel between the sectors during the simulation. At $r = 2a$ we find $aV_0 = 0.0445(3)$ and $aV_1 = 0.498(6)$, i.e. a level splitting of $a\Delta E = 0.454(6)$, which corresponds to about 880 MeV. In addition the ground state hardly rises with r, $aV_0(a) = 0.040$ and $aV_0(2a) = 0.045$, compared to 0.059 and 0.136 in the long directions. So along the deconfined direction no linearly rising flux tube forms and the potential is flattened. In contrast to $l = 8a$ and $l = 6a$, both levels lie far away from the dashed unmixed energies, with V_0 below and V_1 above them. Qualitatively this is the behaviour of the two-level model of section 2.5 with a mixing strength $a\delta = \frac{a\Delta E}{2} \approx 0.23$. A quantitative comparison is not possible with the unmixed energies of the long directions, as those along the deconfined direction differ from them (see chapter 5 for a way to determine them).

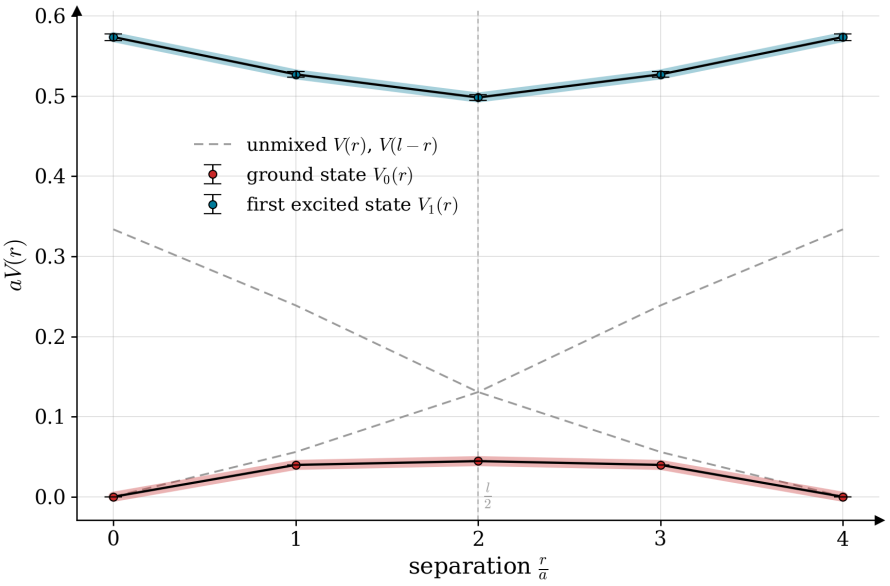


Figure 4.2.3: Ground state $V_0(r)$ and first excited state $V_1(r)$ along the shortened direction for $l = 4a$ (cold start). The dashed lines are the unmixed energies $V(r)$ and $V(l-r)$ of the long direction. The mixing of the direct and the wrapped state leads to an avoided level crossing at $r = \frac{l}{2}$.

4.3. The Level Splitting at $r = \frac{l}{2}$

Figure 4.3.1 summarizes the level splitting $\Delta E\left(\frac{l}{2}\right)$ for the three extents. For $l = 8a$ and $l = 6a$ the splitting is small $a\Delta E \lesssim 0.04$, while for $l = 4a$ it jumps to $a\Delta E = 0.454(6)$. This agrees with the critical couplings of chapter 3, as only $l = 4a$ lies in the deconfined phase. With three extents we can only locate the critical extent between $4a$ and $6a$. Using $a\sqrt{\sigma} = 0.2673(15)$ at $\beta = 2.40$ and $\frac{T_c}{\sqrt{\sigma}} = 0.694(18)$ [22], we get $l_c = \frac{1}{T_c} \approx 5.4a$. So $l = 6a$ corresponds to $\frac{T}{T_c} \approx 0.9$ and lies just below the transition, which agrees with our findings.

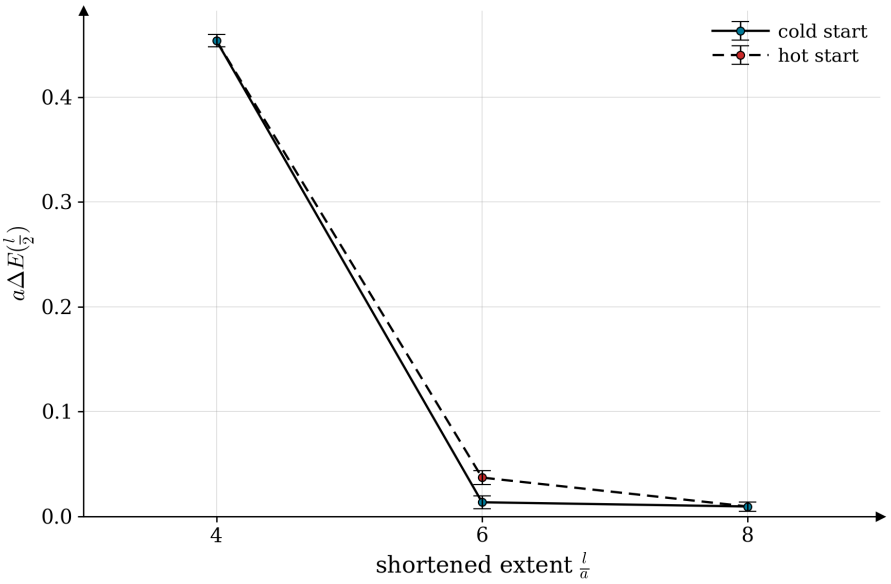


Figure 4.3.1: Level splitting $\Delta E\left(\frac{l}{2}\right) = V_1\left(\frac{l}{2}\right) - V_0\left(\frac{l}{2}\right)$ as a function of the shortened extent l. The hot start is only available for $l = 6a$.

4.4. The Excited State at Large Extents

Finally we consider the long direction y with the extent $24a$, which is equivalent to x, shown in figure 4.4.1 for the $l = 6a$ run. The ground state rises linearly with r up to $r = 12a$, as expected in the confined phase. Its slope at large r is slightly too large, as the plateau fit starting at $t = 3a$ does not fully suppress excited states there (see section 3.3). At $r = 12a$ both levels agree within errors, $aV_0 = 1.05(3)$ and $aV_1 = 1.08(3)$, so also the long direction shows a sharp level crossing, as expected for the unbroken center symmetry.

For small separations the first excited state has large errors, since the wrapped string $V(24a - r)$ is large and its correlator decays quickly. At $r = 3a$ we find $aV_1 = 1.95(30)$. For $r \leq 2a$ the first excited state decreases again, which resembles the sketch in figure 2.5.3, but within the large errors this is not significant. As discussed in section 2.5.3, our operators hardly overlap with glueball states or flux loops winding around the shortened direction, so the first excited state is still dominated by the wrapped string and we do not resolve these states.

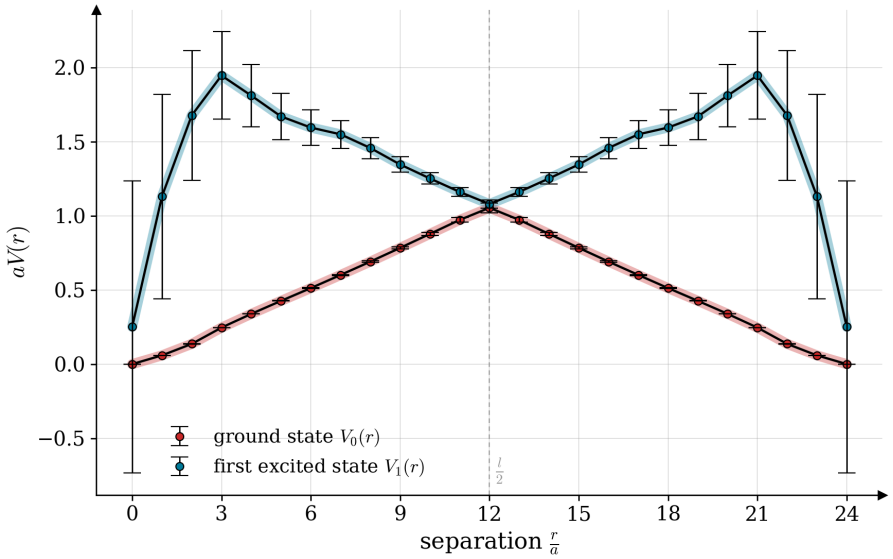


Figure 4.4.1: Ground state $V_0(r)$ and first excited state $V_1(r)$ along the long direction y with extent $24a$ ($l = 6a$, cold start).

Chapter 5

Conclusion and Outlook

5.1. Conclusion

In this thesis we studied the two lowest energy levels of a static $Q\bar{Q}$ pair in SU(2) lattice Yang-Mills theory at the inverse gauge coupling $\beta = 2.40$, with the lattice spacing a, where one spatial extent l is shortened to $8a$, $6a$ and $4a$. In this periodic lattice the flux tube can connect the pair either directly or by wrapping around the shortened direction. We built a 2×2 correlation matrix from the direct and the wrapped Wilson line and extracted the ground state $V_0(r)$ and the first excited state $V_1(r)$ by solving a generalized eigenvalue problem.

The central question was whether and how the direct and the wrapped state mix. The answer is given by the center symmetry of the gauge group, whose breaking signals deconfinement. As predicted in section 2.4.3, the off-diagonal elements of the correlation matrix fluctuate around zero in the confined phase for $l = 8a$, while they are large, $C_{12}(0) \approx 0.64$, in the deconfined phase for $l = 4a$. Therefore the two states do not mix for $l = 8a$ and the levels cross sharply at $r = \frac{l}{2}$, with a remaining splitting $a\Delta E = 0.009(4)$ of the size expected from statistical fluctuations of degenerate levels. For $l = 4a$ the two states mix and we find a clear avoided level crossing with $a\Delta E = 0.454(6)$, i.e. about 880 MeV. In addition, the ground state along the deconfined direction hardly rises with the separation r, so no linearly rising flux tube forms there. For $l = 6a$, which according to the literature value $l_c \approx 5.4a$ lies close to the critical temperature, the splitting is small, but the runs from a hot and a cold start of the heatbath algorithm differ by about 2.5 standard deviations. For purely statistical fluctuations such a difference occurs only in about 1 % of the cases. Both runs spend long stretches in one of the two sectors, so that we cannot decide whether the splitting vanishes. With our three extents we can therefore only locate the critical extent between $4a$ and $6a$. Along the long directions we find a sharp level crossing at $r = 12a$ as well, as expected for the unbroken center symmetry, but we do not resolve glueball states or flux loops winding around the shortened direction at small separations.

These results are subject to some limitations. We use a single lattice spacing and 111 configurations per run without binning, so that the errors for $l = 6a$ are underestimated. The plateau fit starting at the time separation $t = 3a$ biases the potential upwards at large separations, but the level splittings at $r = \frac{l}{2} \leq 4a$ are stable under a later start. For $r \leq 2a$ the energies are lowered by the HYP smearing of

the temporal links. Our operator basis only contains the direct and the wrapped Wilson line, so states with a small overlap with both, like the $Q\bar{Q}$ pair together with a glueball, are not resolved.

5.2. Outlook

The first step is a more careful treatment of our order parameter, the expectation value $\langle P \rangle$ of the Polyakov loop. On a finite lattice $\langle P \rangle$ strictly vanishes even in the deconfined phase, since configurations in both sectors contribute with equal weight. In the Monte Carlo history, the Polyakov loop then resembles a random telegraph signal between $+|P|$ and $-|P|$, where the time it stays in one sector grows with the volume and the temperature. Only for infinitely long runs does its average vanish, while in the infinite volume limit the system remains in one sector. Using $\langle |P| \rangle$ instead, together with its susceptibility, would allow us to locate the critical extent more precisely, and in the same way $\langle |C_{12}| \rangle$ for the off-diagonal elements. In addition the configurations could be separated by the sign of the Polyakov loop, or the wrapped Wilson line could be multiplied by this sign on every configuration, so that the level splitting is determined consistently within one sector. This could clarify the difference between the hot and the cold start for $l = 6a$.

To resolve the transition itself, more extents between $4a$ and $6a$ as well as longer runs with binning are needed. As the transition is of second order for SU(2), we expect the mixing strength δ and thereby the level splitting to grow continuously from zero above the critical temperature. The mixing can also be determined for all separations from the eigenvectors of the GEVP. After orthonormalizing the trial states, they give the mixing angle $\theta(r)$ of the direct and the wrapped state, from which the mixing strength $\delta(r) = \frac{1}{2}\Delta E \sin 2\theta$ and the unmixed energies along the shortened direction follow. This would allow a quantitative comparison with the two-level model of section 2.5. For SU(3) with the center symmetry Z_3 the transition is of first order, so that the splitting might jump at the critical temperature instead. Further lattice spacings would allow us to extrapolate the splitting to the continuum and to give the results in physical units without relying on a single value of a. Finally, a larger operator basis, e.g. with several smearing levels or glueball operators, and a later start of the plateau fit would improve the excited state and could resolve the thresholds at small separations.

Appendix A

Thermalization

To check whether the Markov chain has reached equilibrium, we monitor the average plaquette $\langle U_P \rangle$ after every sweep. Figure A.0.1 shows its Monte Carlo history for all runs on a logarithmic sweep axis. The cold starts begin at $\langle U_P \rangle \approx 0.72$ and the hot start at $\langle U_P \rangle \approx 0.40$, but both approach the same value within about 10 and 30 sweeps, respectively. So the $N_{therm} = 300$ discarded sweeps are safely sufficient for the plaquette. After thermalization we find $\langle U_P \rangle = 0.6301$ for $l = 8a$, 0.6300 for both starts with $l = 6a$ and 0.6319 for $l = 4a$, with fluctuations of about 0.0007 between successive sweeps. The slightly larger value for $l = 4a$ reflects the deconfined shortened direction. As the plaquette is a local observable, it thermalizes and decorrelates quickly and is therefore not sensitive to the slow dynamics close to the critical temperature.

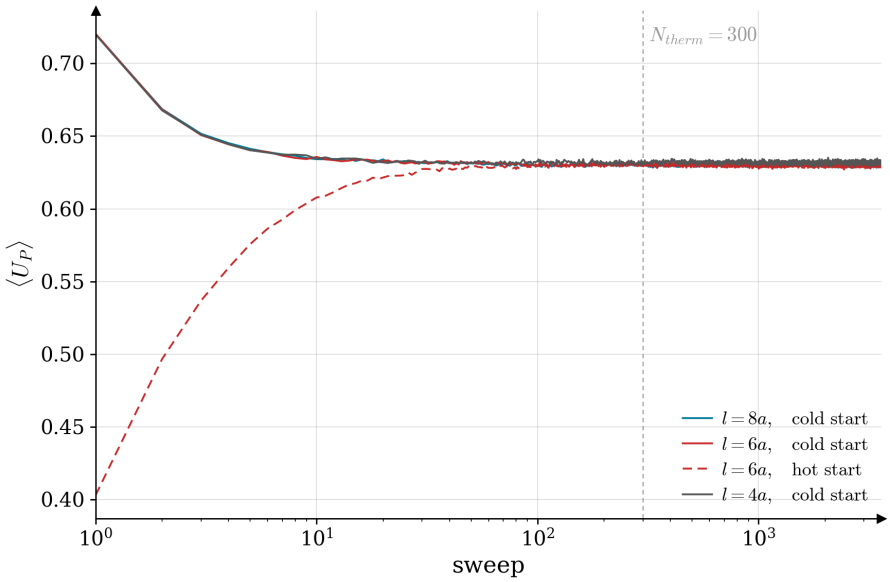
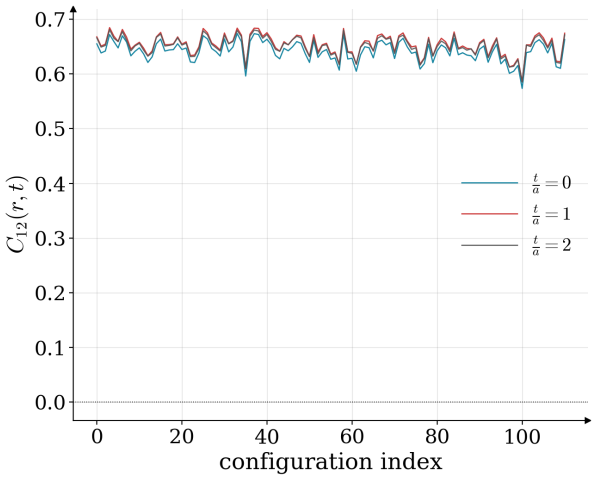
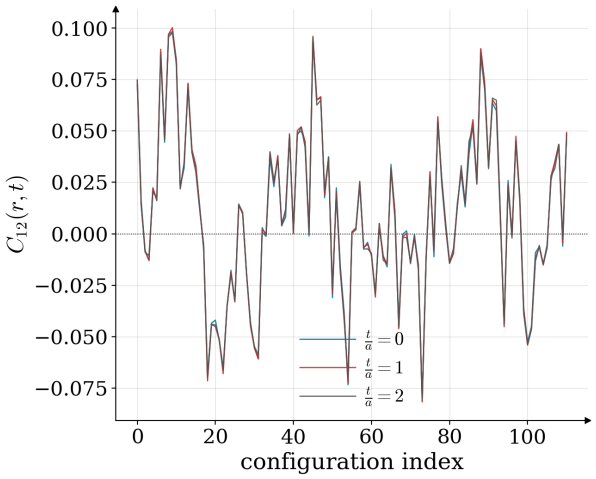


Figure A.0.1: Monte Carlo history of the average plaquette for all runs. The dashed line marks the $N_{therm} = 300$ discarded sweeps.

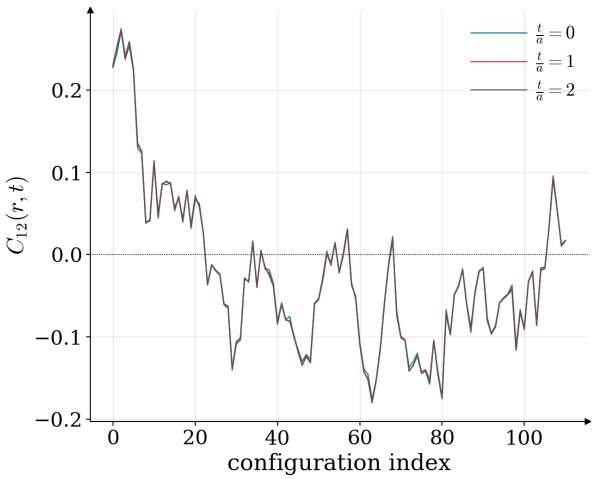
Besides the plaquette we monitor the Polyakov loop along the shortened direction. It is given by the off-diagonal element $C_{12}(t = 0)$, since for $t = 0$ the direct and the wrapped Wilson line together wind exactly once around the shortened direction. Figure A.0.2 shows its Monte Carlo history for the three extents l. For $l = 4a$ the Polyakov loop fluctuates around 0.64 and stays positive on all configurations, so the system remains in one sector of the deconfined phase, as tunnelling between the sectors is strongly suppressed. For $l = 8a$ it fluctuates around zero, as expected in the confined phase. For $l = 6a$ neither run fluctuates around zero on short scales. The cold start begins at about 0.25, drops within the first 20 measurements and then stays around -0.1 for most of the run. The hot start first fluctuates around zero, but then remains at positive values up to about 0.25 from configuration 30 to 74, before it returns to negative values. So both runs spend long stretches in one of the two sectors, with a mean of -0.03 for the cold and $+0.06$ for the hot start. This slow decorrelation reflects that $l = 6a$ lies close to the critical temperature, so that both runs should be interpreted with care.



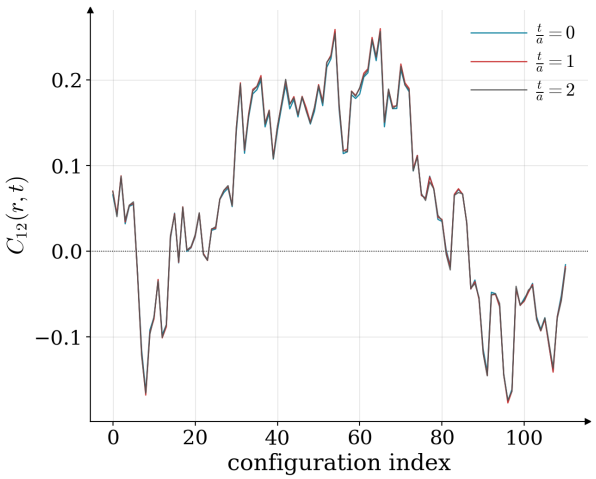
(a) $l = 4a$, cold start



(b) $l = 8a$, cold start



(c) $l = 6a$, cold start



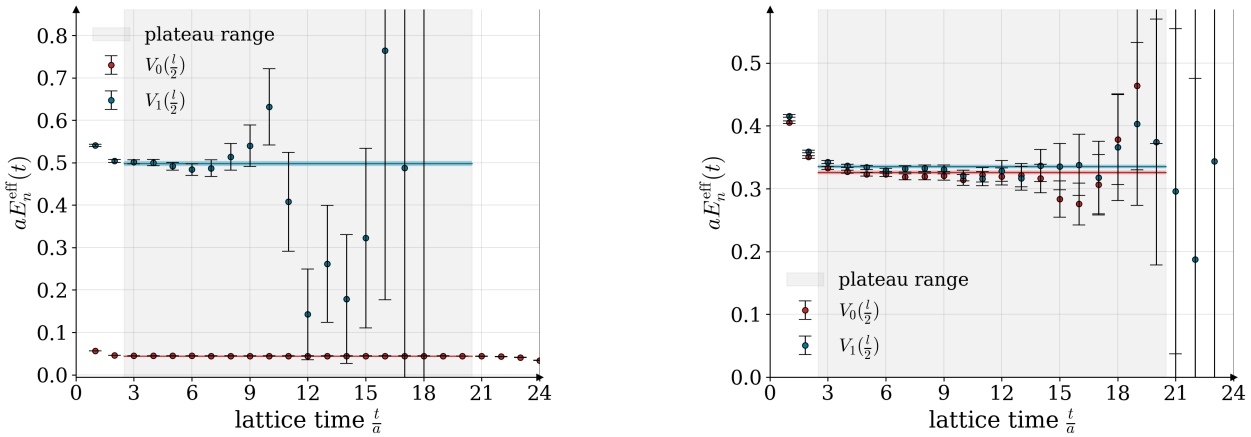
(d) $l = 6a$, hot start

Figure A.0.2: Monte Carlo history of the off-diagonal element $C_{12}(t)$ at $r = a$ along the shortened direction. The curve for $t = 0$ is the Polyakov loop around the shortened direction, the curves for $t = a$ and $t = 2a$ follow it closely.

Appendix B

Effective Energy Plateaus

Figure B.0.1 shows the effective energies $E_n^{\text{eff}}(t)$ of the projected correlators at $r = \frac{l}{2}$ for the deconfined extent $l = 4a$ and the confined extent $l = 8a$. The shaded region marks the plateau range $3a \leq t \leq 20a$, the horizontal lines with bands are the fitted energies with their jackknife errors. For $l = 4a$ the ground state forms a clean plateau from $t = 3a$ on over the whole range. The first excited state has a plateau for $3a \leq t \lesssim 8a$, after which its correlator is dominated by noise. Due to the weights of the plateau fit the result $aV_1 = 0.498(6)$ is determined by the precise points at small t. For $l = 8a$ both levels are almost degenerate and form plateaus from $t = 3a$ on, the points at $t \gtrsim 15a$ fluctuate strongly but contribute little to the fit. At $t = 3a$ the points still lie slightly above the plateau, which reflects the remaining excited state contamination discussed in section 3.3.



(a) $l = 4a$, cold start

(b) $l = 8a$, cold start

Figure B.0.1: Effective energies $E_n^{\text{eff}}(t)$ of the ground state and the first excited state at $r = \frac{l}{2}$ along the shortened direction. The shaded region marks the plateau range $3a \leq t \leq 20a$, the horizontal lines and bands the fitted energies with their jackknife errors.

Bibliography

[1] Michael Creutz (1980): "*Monte Carlo Study of Quantized SU(2) Gauge Theory*", Phys. Rev. D **21**, 2308–2315, doi:10.1103/PhysRevD.21.2308

[2] Christof Gattringer, Christian B. Lang (2010): "*Quantum Chromodynamics on the Lattice — An Introductory Presentation*", Lecture Notes in Physics **788**, Springer-Verlag, doi:10.1007/978-3-642-01850-3

[3] Estia Eichten, Kurt Gottfried, Toichiro Kinoshita, Kenneth D. Lane, Tung-Mow Yan (1980): "*Charmonium: Comparison with Experiment*", Phys. Rev. D **21**, 203, doi:10.1103/PhysRevD.21.203

[4] Larry D. McLerran, Benjamin Svetitsky (1981): "*Quark Liberation at High Temperature: A Monte Carlo Study of SU(2) Gauge Theory*", Phys. Rev. D **24**, 450, doi:10.1103/PhysRevD.24.450

[5] Janos Polonyi, Kornel Szlachanyi (1982): "*Phase Transition from Strong Coupling Expansion*", Phys. Lett. B **110**, 395–398, doi:10.1016/0370-2693(82)91280-1

[6] Jens Langelage, Stefano Lottini, Owe Philipsen (2011): "*Centre symmetric 3d effective actions for thermal SU(N) Yang-Mills from strong coupling series*", JHEP **02**, 057, doi:10.1007/JHEP02(2011)057

[7] Owe Philipsen (2012): "*Effective theory for QCD at finite temperature and density from strong coupling expansion*", PoS(QCD-TNT-II)035, pos.sissa.it/136/035

[8] Benjamin Svetitsky, Laurence G. Yaffe (1982): "*Critical Behavior at Finite Temperature Confinement Transitions*", Nucl. Phys. B **210**, 423–447, doi:10.1016/0550-3213(82)90172-9

[9] John von Neumann, Eugene Wigner (1929): "*Über das Verhalten von Eigenwerten bei adiabatischen Prozessen*", Physikalische Zeitschrift **30**, 467–470

[10] Owe Philipsen, Hartmut Wittig (1998): "*String breaking in non-Abelian gauge theories with fundamental matter fields*", Phys. Rev. Lett. **81**, 4056–4059, doi:10.1103/PhysRevLett.81.4056

[11] SESAM Collaboration, Gunnar S. Bali, Hartmut Neff, Thomas Düssel, Thomas Lippert, Klaus Schilling (2005): "*Observation of string breaking in QCD*", Phys. Rev. D **71**, 114513, doi:10.1103/PhysRevD.71.114513

[12] Kenzo Ishikawa, Gerrit Schierholz, Michael Teper (1983): "*Calculation of the glueball mass spectrum of SU(2) and SU(3) non-abelian lattice gauge theories I: Introduction and SU(2)*", Z. Phys. C **19**, 327–352, doi:10.1007/BF01577189

[13] Biagio Lucini, Michael Teper, Urs Wenger (2004): "*Glueballs and k-strings in SU(N) gauge theories: calculations with improved operators*", JHEP **06**, 012, doi:10.1088/1126-6708/2004/06/012

[14] Christopher Michael, G. A. Tickle, Michael J. Teper (1988): "*The SU(2) Glueball Spectrum in a Small Volume*", Phys. Lett. B **207**, 313–318, doi:10.1016/0370-2693(88)90582-5

[15] K. Jimmy Juge, Julius Kuti, Colin Morningstar (2003): "*Fine structure of the QCD string spectrum*", Phys. Rev. Lett. **90**, 161601, doi:10.1103/PhysRevLett.90.161601

[16] Jochen Fingberg, Urs M. Heller, Frithjof Karsch (1993): "*Scaling and Asymptotic Scaling in the SU(2) Gauge Theory*", Nucl. Phys. B **392**, 493–517, arXiv:hep-lat/9208012

[17] Anna Hasenfratz, Francesco Knechtli (2001): "*Flavor symmetry and the static potential with hypercubic blocking*", Phys. Rev. D **64**, 034504, doi:10.1103/PhysRevD.64.034504

[18] Michele Della Morte, Andrea Shindler, Rainer Sommer (2005): "*On lattice actions for static quarks*", JHEP **08**, 051, doi:10.1088/1126-6708/2005/08/051

[19] APE Collaboration, M. Albanese et al. (1987): "*Glueball Masses and String Tension in Lattice QCD*", Phys. Lett. B **192**, 163–169, doi:10.1016/0370-2693(87)91160-9

[20] Martin Lüscher, Ulli Wolff (1990): "*How to Calculate the Elastic Scattering Matrix in Two-dimensional Quantum Field Theories by Numerical Simulation*", Nucl. Phys. B **339**, 222–252, doi:10.1016/0550-3213(90)90540-T

[21] Benoit Blossier, Michele Della Morte, Georg von Hippel, Tereza Mendes, Rainer Sommer (2009): "*On the generalized eigenvalue method for energies and matrix elements in lattice field theory*", JHEP **04**, 094, doi:10.1088/1126-6708/2009/04/094

[22] Michael J. Teper (1998): "*Glueball masses and other physical properties of SU(N) gauge theories in D = 3+1: a review of lattice results for theorists*", arXiv:hep-th/9812187

[23] Constantin Bachas (1986): "*Convexity of the Quarkonium Potential*", Phys. Rev. D **33**, 2723, doi:10.1103/PhysRevD.33.2723

[24] Rainer Sommer (1994): "*A New way to set the energy scale in lattice gauge theories and its applications to the static force and α_s in SU(2) Yang-Mills theory*", Nucl. Phys. B **411**, 839–854, doi:10.1016/0550-3213(94)90473-1

[25] Owe Philipsen, Marc Wagner (2014): "*On the definition and interpretation of a static quark anti-quark potential in the colour-adjoint channel*", Phys. Rev. D **89**, 014509, doi:10.1103/PhysRevD.89.014509